Counterdiabatic transfer of a quantum state in a tunable Heisenberg spin chain via the variational principle

Yunlan Ji [⊙],[1] Feifei Zhou [⊙],[1] Xi Chen,[2] Ran Liu [⊙],[3,4,5] Zhaokai Li,[3,4,5] Hui Zhou [⊙],[1,6,*] and Xinhua Peng[3,4,5,†]

[1]*School of Physics, Hefei University of Technology, Hefei, Anhui 230009, China*
[2]*Department of Physics, The Hong Kong University of Science and Technology, Clear Water Bay, Kowloon, Hong Kong, China*
[3]*Hefei National Laboratory for Physical Sciences at the Microscale and Department of Modern Physics,*
University of Science and Technology of China, Hefei 230026, China
[4]*CAS Key Laboratory of Microscale Magnetic Resonance, University of Science and Technology of China, Hefei 230026, China*
[5]*Synergetic Innovation Center of Quantum Information and Quantum Physics,*
University of Science and Technology of China, Hefei 230026, China
[6]*Department of Physics, Shaanxi University of Science and Technology, Xi'an 710021, China*

We present a couple of counterdiabatic (CD) schemes for a rapid and high-fidelity transfer of quantum state across a one-dimensional spin chain, between two weakly coupled external qubits at each end. Employing the effective low-energy Hamiltonian of the system, we first construct the optimal CD terms based on the variational principle and then put forward two experimentally feasible shortcuts, which only need to manipulate couplings between the external qubits and chain. Compared to traditional adiabatic protocol, the resulting schemes allow a drastic increase in state-transfer fidelity in a short time. Furthermore, numerical simulation demonstrates that our speed-up protocols hold robustness against the imperfections of control fields and evolution time. The proposed schemes may be applicable to fast quantum-information transport in various spin-based physical systems.

I. INTRODUCTION

Faithful and fast transfer of quantum information between two different systems is necessary for scalable quantum information processing [1,2]. For short-distance quantum state transfer (QST), spin chains are paradigmatic systems due to native spin-spin interactions and simple physical encodings [3–9]. Many established schemes, which depend on precisely engineering couplings among qubits and dynamical evolution time, are usually vulnerable to environmental noises, time errors, and so on. To mitigate this drawback, the adiabatic control (a technique carries the advantage of inherent robustness to pulse errors and noise) can be adopted, and it has emerged as an appealing route to realize QST [10–16]. Nevertheless, such controls typically achieve high-fidelity state transfer at the cost of time, and thus, may suffer from decoherence in a quantum system.

To speed up the quantum adiabatic processes, the technique termed shortcut to adiabaticity (STA) [17–19] was put forward, which provides a powerful method of accelerating quantum-information processing and inheriting the robustness of adiabatic dynamics. Till now, STA has great applications in many fields (see recent reviews in Refs. [20,21]), one of which is fast quantum state transport in arrays of spin qubits [22–30]. For example, the authors of Ref. [22] constructed superadiabatic QST passage in an odd-size spin chain, which

exploited CD driving and unitary transformation on the simplified Hamiltonian. The authors of Ref. [25] proposed a high-fidelity STA protocol for state transfer via quantum Zeno dynamics and inverse Hamiltonian engineering. By means of the approximate mapping between the spin chain and a single particle in a harmonic potential, the authors of Ref. [29] designed a scheme for fast and robust magnon transport in a spin chain.

Among the known methods to construct STA, CD driving provides a quite simple way to exactly suppress nonadiabatic transitions by adding a CD term to the original Hamiltonian [17,18]. However, the main challenge of obtaining CD term is to diagonalize the Hamiltonian in the full Hilbert space, which hinders its access to practical implementations for many-body systems [31–34]. Recently, a variational method [35,36], taking available resources and experimental constraints into consideration, was proposed to obtain the best possible CD term approximatively. It can nullify the need for exact diagonalization of the system. Some very recent efforts were devoted to exploring its potential applications, ranging from quantum chaos and phase transition [37,38] to quantum annealing of many-body systems [39–42] and fast control of complicated quantum systems [43–46].

Inspired by the variational principle to CD driving, here we put forward two high-fidelity and minimal-control protocols to transfer quantum state across a Heisenberg spin-$1/2$ chain, which make time significantly shorter than that using the adiabatic schemes. The rest of the paper is organized as follows. In Sec. II we briefly review the variational principle to CD driving and introduce the physical system, a strongly

*zhouhui9240@163.com
†xhpeng@ustc.edu.cn

coupled Heisenberg chain with an odd number of spins, to perform the adiabatic state transfer protocol. In Sec. III, we utilize the variational strategy in the simplified Hamiltonian to design the optimal CD drivings with different auxiliary operators, without resorting to diagonalizing the instantaneous Hamiltonian. Subsequently, combining the results with Floquet driving and unitary transformation, two high-fidelity and feasible shortcuts for diabatic QST are constructed. The effectiveness of these protocols is reported in Sec. IV, where we also investigate their robustness against the errors from control fields and evolution time. Finally, a brief summary is presented in Sec. V.

II. PRELIMINARIES

Consider a quantum system consisting of sender, channel, and receiver subsystems, our goal is to transport a quantum state from the sender to the receiver quickly. In what follows, we will briefly introduce the method and system involved. For convenience, we set $\hbar = 1$ and express the time-dependent parameters implicitly unless necessary.

A. Variational method to CD driving

To counteract the possible transitions when the adiabatic driving of a system $H_0(\lambda)$ is speeded up, we can drive the system with the CD protocol [17,18]

$$H(\lambda) = H_0(\lambda) + \dot{\lambda} \mathcal{A}_\lambda, \tag{1}$$

where λ is a time-dependent parameter, $\mathcal{A}_\lambda$ is the adiabatic gauge potential (AGP) [35], and the dot denotes the time derivative. Thus, the well-designed system will follow the time-dependent eigenstates of H_0 from beginning to end without requiring slow driving. In many-body systems, however, it is hard to acquire the exact $\mathcal{A}_\lambda$ since it usually requires spectral information of the Hamiltonian at any time.

To avoid this problem, a variational ansatz to optimally approximate the AGP (or CD term) was proposed in Refs. [35,36]. Provided there exists a trial AGP $\mathcal{A}_\lambda^*$ consisting of allowed operators in practice, e.g., single-spin terms and two-body interactions, the optimal approximation can be built by finding the minimum operator distance

$$D^2(\mathcal{A}_\lambda^*) = \mathrm{Tr}\{[G_\lambda(\mathcal{A}_\lambda) - G_\lambda(\mathcal{A}_\lambda^*)]^2\}, \tag{2}$$

where the Hermitian operator G_λ is defined as

$$G_\lambda(\mathcal{X}_\lambda) \equiv \partial_\lambda H_0 + i[\mathcal{X}_\lambda, H_0]. \tag{3}$$

Furthermore, this process is equivalent to minimizing the Hilbert-Schmidt norm of the operator $G_\lambda(\mathcal{A}_\lambda^*)$

$$\mathcal{S}(\mathcal{A}_\lambda^*) = \mathrm{Tr}[G_\lambda^2(\mathcal{A}_\lambda^*)], \tag{4}$$

with respect to $\mathcal{A}_\lambda^*$. In this way, the demand for diagonalizing Hamiltonian H_0 can be eliminated. For a detailed derivation, please see Ref. [35]. However, there exists a potential problem to choose the variational basis from available operators beforehand since the number of possible operators increases exponentially with system size. Recently, in Ref. [43] Claeys *et al.* demonstrated that the approximated A_λ^* could be constructed from a series of nested commutators of H_0
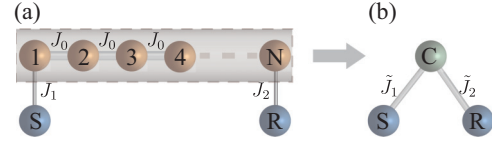

FIG. 1. Schematic of the spin structure. (a) Two external qubits S and R (blue balls) weakly coupled to an odd-size spin chains (yellow balls), namely $J_{1,2} \ll J_0$. (b) The corresponding effective model in the low-energy subspace. The odd-size spin chain in its ground state works as an effective $1/2$ spin, labeled as C (brown ball) and $\tilde{J}_{1,2}(t)$ denote the effective qubit-chain couplings.

and $\partial_\lambda H_0$,

$$[H_0(\lambda), [H_0(\lambda), \ldots, [H_0(\lambda), \partial_\lambda H_0(\lambda)]]], \tag{5}$$

where the number of $H_0(\lambda)$ in the commutation relation is odd. Generally speaking, higher-order commutators can provide more basis operators and benefit a better approximation of AGP in many-body systems. In virtue of simplicity and efficiency, the variational principle to CD driving with the nested commutator ansatz was further explored in the p-spin model [40] and the honeycomb Kitaev model [46].

B. Model and adiabatic QST protocol

As paradigmatic systems, spin chains were extensively studied in the areas of statistical physics and quantum information processing, e.g., short-distance QST. Here the composite system we consider is the spin chain of the Heisenberg type, which has been experimentally realized in quantum dots [47], ultracold atoms [48], and Josephson junction arrays [49]. As illustrated in Fig. 1(a), two external qubits, served as the sender and receiver (labeled as S and R, respectively), weakly couple to an odd-size Heisenberg spin chain (labeled from 1 to N) at both ends. The Hamiltonian is written as

$$H_0 = J_1 \, \boldsymbol{\sigma}_S \cdot \boldsymbol{\sigma}_1 + J_0 \sum_{i=1}^{N-1} \boldsymbol{\sigma}_i \cdot \boldsymbol{\sigma}_{i+1} + J_2 \, \boldsymbol{\sigma}_N \cdot \boldsymbol{\sigma}_R. \tag{6}$$

Here $\boldsymbol{\sigma} = (\sigma^x, \sigma^y, \sigma^z)$ denote the Pauli matrices acting on each spin, and J_0 represents the uniform nearest-neighbor couplings of the spin chain, which is much larger than the qubit-chain couplings $J_{1,2}$. Since H_0 commutes with the z component of the total spin operator, the number of excitations in the QST process is preserved.

To adiabatically transfer a quantum state from the sender to receiver, according to Ref. [22] we start with the initial state

$$|\Psi(0)\rangle = |\psi_0\rangle \otimes |\psi_g\rangle,$$

where $|\psi_0\rangle = a|0\rangle + b|1\rangle$ with a and b being arbitrary coefficients represents the quantum state to-be-transported, and $|\psi_g\rangle$ represents the ground state of the rest subsystems. Accordingly, the target state can be transferred to the receiver by adiabatically switching the time-dependent qubit-chain couplings $J_{1,2}(t)$ from

$$J_1(0) = 0, \quad J_2(0) = J_R, \tag{7}$$

to

$$J_1(T) = J_L, \quad J_2(T) = 0, \tag{8}$$

during which J_0 keeps constant. Here we set the parameters $J_{L,R} = 1$ with no loss of generality, and in the following we randomly choose $a = e^{-i\frac{2\pi}{3}} \sin \frac{2\pi}{9}$, $b = \cos \frac{2\pi}{9}$ for convenience of numerical simulation. The final quality of QST can be assessed by performing quantum state tomography on the receiver qubit. Since the minimal energy gap of this system tends to zero with the growth of system size [4], i.e., $\Delta \propto \frac{1}{N}$, the time needs to satisfy the adiabatic condition will increase ($T \gg 1/\Delta$). In the following sections, by simplifying the dynamics of the system, we will construct two feasible schemes for accelerating the adiabatic state transfer via the variational method.

III. COUNTERDIABATIC TRANSFER OF QUANTUM STATE VIA THE VARIATIONAL PRINCIPLE

The odd-size Heisenberg spin-1/2 chain has two-fold degenerate ground states $\{|0_C\rangle, |1_C\rangle\}$ and behaves like a central spin at the low energies [4,50,51] when two marginal qubits are weakly coupled to this chain, i.e., $J_{1,2} \ll J_0$, as shown in Fig. 1(b). According to the perturbed theory, the effective Hamiltonian to first order is given by

$$\mathcal{H}_0 = \tilde{J}_1 \boldsymbol{\sigma}_S \cdot \boldsymbol{\sigma}_C + \tilde{J}_2 \boldsymbol{\sigma}_C \cdot \boldsymbol{\sigma}_R, \tag{9}$$

where the central spin operator $\boldsymbol{\sigma}_C$ is defined by $\sigma_C^x = |0_C\rangle\langle 1_C| + |1_C\rangle\langle 0_C|$, $\sigma_C^y = -i|0_C\rangle\langle 1_C| + i|1_C\rangle\langle 0_C|$ and $\sigma_C^z = |0_C\rangle\langle 0_C| - |1_C\rangle\langle 1_C|$. The effective couplings $\tilde{J}_{1,2}(t)$ are proportional to the dimensionless local magnetic moments of the first and end spins of the chain in the ground state [4,50,51], which read

$$\tilde{J}_1 = J_1 \langle 0_C | \sigma_1^z | 0_C \rangle, \quad \tilde{J}_2 = J_2 \langle 0_C | \sigma_N^z | 0_C \rangle. \tag{10}$$

It means QST in an odd-size chain (6) can be explored in the light of the effective Hamiltonian (9) qualitatively. Since $\tilde{J}_{1,2}$ can be always rescaled by the factor $m = \langle 0_C | \sigma_{1,N}^z | 0_C \rangle$, we will take $m = 1$ in this effective three-spin model unless it is mapped back to the whole spin chain. For brevity, we will use the subscripts $\{1, 2, 3\}$ to label the three spins in Fig. 1(b).

Substituting Eq. (9) into the different-order commutation relation of Eq. (5), the results show that the following operators $\{\mathcal{O}_k (k = 1, \ldots, 6)\} = \{\sigma_1^x \sigma_2^y \sigma_3^z, \sigma_1^y \sigma_2^x \sigma_3^z, \sigma_1^x \sigma_2^z \sigma_3^y, \sigma_1^y \sigma_2^z \sigma_3^x, \sigma_1^z \sigma_2^x \sigma_3^y, \sigma_1^z \sigma_2^y \sigma_3^x\}$ can work as the possible variational basis. Hence, the trial gauge potential $\mathcal{A}^*$ can be constructed as

$$\mathcal{A}^* = i \sum_{k=1}^{6} \beta_k \mathcal{O}_k, \tag{11}$$

with β_k being variational coefficient. To preserve the excitations in the QST, $\mathcal{A}^*$ needs to fulfill the condition $[\mathcal{A}^*, \sum \sigma_i^z] = 0$, which results in the following constraints:

$$\beta_1 = -\beta_2, \quad \beta_3 = -\beta_4, \quad \beta_5 = -\beta_6. \tag{12}$$

Put it in another way, the possible operators $\{\mathcal{O}_k\}$ can be recombined as

$$\begin{aligned}
\mathcal{L}_1 &= \sigma_1^x \sigma_2^y \sigma_3^z - \sigma_1^y \sigma_2^x \sigma_3^z, \\
\mathcal{L}_2 &= \sigma_1^z \sigma_2^x \sigma_3^y - \sigma_1^z \sigma_2^y \sigma_3^x, \\
\mathcal{L}_3 &= \sigma_1^y \sigma_2^z \sigma_3^x - \sigma_1^x \sigma_2^z \sigma_3^y.
\end{aligned} \tag{13}$$

Then, $\mathcal{A}^*$ can be rewritten as

$$\mathcal{A}^* = i \sum_{k=1}^{3} \alpha_k \mathcal{L}_k. \tag{14}$$

To avoid confusion, here the symbols α_k are used to stand for the undetermined coefficients. Substituting this $\mathcal{A}^*$ into Eq. (3), we have

$$G(\mathcal{A}_\lambda^*) = \sum_{i=1}^{3} \mathcal{D}_i(\alpha_1, \alpha_2, \alpha_3) [\sigma_i^x \sigma_{i+1}^x + \sigma_i^y \sigma_{i+1}^y]$$

$$+ \sum_{i=1}^{3} \mathcal{K}_i(\alpha_1, \alpha_2, \alpha_3) \sigma_i^z \sigma_{i+1}^z, \tag{15}$$

in which $\sigma_1^v = \sigma_4^v$ with $v = x, y, z$, and the time-dependent coefficients $\mathcal{D}_i$, $\mathcal{K}_i$ can be formulated as a matrix

$$\mathcal{D} = \begin{bmatrix} \dot{\tilde{J}}_1 - 2(\alpha_1 + \alpha_3)\tilde{J}_2 \\ \dot{\tilde{J}}_2 + 2(\alpha_2 + \alpha_3)\tilde{J}_1 \\ 2(\alpha_1 + \alpha_3)\tilde{J}_2 - 2(\alpha_2 + \alpha_3)\tilde{J}_1 \end{bmatrix}, \tag{16}$$

and

$$\mathcal{K} = \begin{bmatrix} \dot{\tilde{J}}_1 - 4\alpha_2 \tilde{J}_2 \\ \dot{\tilde{J}}_2 + 4\alpha_1 \tilde{J}_1 \\ 4\alpha_2 \tilde{J}_2 - 4\alpha_1 \tilde{J}_1 \end{bmatrix}. \tag{17}$$

Thus, the Hilbert-Schmidt norm of the operator (15), by virtue of the Pauli matrices being traceless, amounts to adding up squares of coefficients of each spin operator, i.e., $\mathcal{S}(\mathcal{A}_\lambda^*) = 2^3 \sum_{i=1}^{3} (2\mathcal{D}_i^2 + \mathcal{K}_i^2)$, which can be represented as a quadratic form about the variables $\{\alpha_k\}$. Minimizing $\mathcal{S}(\mathcal{A}_\lambda^*)$ with respect to $\{\alpha_k\}$ and leaving out a trivial constant coefficient, we can obtain a linear system of equations

$$\mathbb{M}\vec{c} = \mathcal{Q}, \tag{18}$$

Here $\mathcal{Q} = \tilde{J}_1 \dot{\tilde{J}}_2 - \dot{\tilde{J}}_1 \tilde{J}_2$, the column vectors $\vec{c} = [\alpha_1, \alpha_2, \alpha_3]^T$, and the coefficient matrix $\mathbb{M}$ reads

$$\mathbb{M} = \begin{bmatrix} 8\tilde{J}_1^2 + 4\tilde{J}_2^2 & -6\tilde{J}_1\tilde{J}_2 & 4\tilde{J}_2^2 - 2\tilde{J}_1\tilde{J}_2 \\ -6\tilde{J}_1\tilde{J}_2 & 8\tilde{J}_2^2 + 4\tilde{J}_1^2 & 4\tilde{J}_1^2 - 2\tilde{J}_1\tilde{J}_2 \\ 4\tilde{J}_2^2 - 2\tilde{J}_1\tilde{J}_2 & 4\tilde{J}_1^2 - 2\tilde{J}_1\tilde{J}_2 & 4(\tilde{J}_1^2 + \tilde{J}_2^2 - \tilde{J}_1\tilde{J}_2) \end{bmatrix}. \tag{19}$$

Elements in the kth row of the matrix represent the expansion coefficients of $\frac{\partial \mathcal{S}}{\partial \alpha_k}$ in the bases $\{\alpha_1, \alpha_2, \alpha_3\}$, respectively. Note that if the CD operators in Eq. (13) are partially allowed, i.e., the some coefficient α_m is set to zero beforehand, the corresponding basis α_m of $\vec{c}$ and the elements in both the mth row and mth column of $\mathbb{M}$ will not exist.

Depending on the number of the CD operators included, the optimal variational solutions $\tilde{\alpha}_k(t)$ can be given by solving Eq. (18). We list all the possible solutions, classified into the three conditions, in Table I. The other two solutions in case 2 were ignored due to the infinite couplings near the boundary. Taking all the optimal solutions into consideration, the resulting CD driving Hamiltonian is

$$\mathcal{H}^{(l)} = \mathcal{H}_0 + \mathcal{H}_{cd}^{(l)}, \tag{20}$$

where $\mathcal{H}_{cd}^{(l)} = \sum \tilde{\alpha}_k^{(l)}(t) \mathcal{L}_k$ involves l grouped operators in Eq. (13) with $\tilde{\alpha}_k^{(l)}(t)$ being corresponding coefficients listed

TABLE I. Available solutions to Eq. (18) with the different number of CD operators in Eq. (13). Here the explicit time dependence of $\tilde{J}_1$ and $\tilde{J}_2$ are omitted for clarity.

Case 1	$\alpha_2 = \alpha_3 = 0, \tilde{\alpha}_1^{(1)}(t) = \dfrac{\dot{\tilde{J}}_1 \tilde{J}_2 - \dot{\tilde{J}}_2 \tilde{J}_1}{8\tilde{J}_1^2 + 4\tilde{J}_2^2}; \; \alpha_1 = \alpha_3 = 0, \tilde{\alpha}_2^{(1)}(t) = \dfrac{\dot{\tilde{J}}_1 \tilde{J}_2 - \dot{\tilde{J}}_2 \tilde{J}_1}{4\tilde{J}_1^2 + 8\tilde{J}_2^2}; \; \alpha_1 = \alpha_2 = 0, \tilde{\alpha}_3^{(1)}(t) = -\dfrac{\dot{\tilde{J}}_1 \tilde{J}_2 - \dot{\tilde{J}}_2 \tilde{J}_1}{4(\tilde{J}_1^2 + \tilde{J}_2^2 - \tilde{J}_1 \tilde{J}_2)};$
Case 2	$\alpha_3 = 0, \tilde{\alpha}_1^{(2)}(t) = \dfrac{(\dot{\tilde{J}}_1 \tilde{J}_2 - \dot{\tilde{J}}_2 \tilde{J}_1)(2\tilde{J}_1^2 + 3\tilde{J}_1 \tilde{J}_2 + 4\tilde{J}_2^2)}{16\tilde{J}_1^4 + 22\tilde{J}_1^2 \tilde{J}_2^2 + 16\tilde{J}_2^4}, \tilde{\alpha}_2^{(2)}(t) = \dfrac{(\dot{\tilde{J}}_1 \tilde{J}_2 - \dot{\tilde{J}}_2 \tilde{J}_1)(4\tilde{J}_1^2 + 3\tilde{J}_1 \tilde{J}_2 + 2\tilde{J}_2^2)}{16\tilde{J}_1^4 + 22\tilde{J}_1^2 \tilde{J}_2^2 + 16\tilde{J}_2^4};$
Case 3	$\tilde{\alpha}_1^{(3)}(t) = \tilde{\alpha}_2^{(3)}(t) = \tilde{\alpha}_3^{(3)}(t) = \tilde{\alpha}^{(3)} = \dfrac{\dot{\tilde{J}}_1 \tilde{J}_2 - \dot{\tilde{J}}_2 \tilde{J}_1}{8(\tilde{J}_1^2 - \tilde{J}_1 \tilde{J}_2 + \tilde{J}_2^2)};$

in Table I. In this simplified three-spin model, the effective initial state is

$$|\Phi(0)\rangle = (a|0\rangle + b|1\rangle) \otimes \frac{|01\rangle - |10\rangle}{\sqrt{2}}. \qquad (21)$$

A general solution of the Schrödinger equation is

$$|\Phi(t)\rangle = \mathcal{T} \exp\left[-i \int_0^T \mathcal{H}^{(l)}(t) dt\right] |\Phi(0)\rangle, \qquad (22)$$

with $\mathcal{T}$ and T being the time-ordering operator and total evolution time, respectively.

Figure 2 shows the instantaneous fidelity $F(t)$ of the evolved state $|\Phi(t)\rangle$ with the ground state of $\mathcal{H}_0(t)$ when different variational-based CD protocols are taken into account. Since there exist two degenerate ground states $|\Phi_g^{\pm}(t)\rangle$, $F(t)$ is defined as

$$F(t) = |\langle \Phi_g^-(t)|\Phi(t)\rangle|^2 + |\langle \Phi_g^+(t)|\Phi(t)\rangle|^2. \qquad (23)$$

We can see that utilizing full set of the CD operators in Eq. (13), i.e., $\mathcal{H}_{cd}^{(3)} = \sum_{k=1}^3 \tilde{\alpha}_k^{(3)}(t) \mathcal{L}_k$, can keep the system in the ground states completely (blue solid line). By contrast, in the same situation using the native protocol leads to the fidelity only about 0.45 at the final time (black dotted line). If we increase the number of CD operators, the fidelity will be significantly improved. For instance, employing two CD
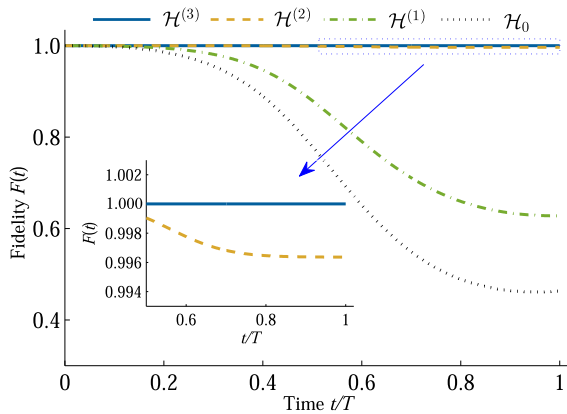

FIG. 2. Instantaneous fidelity $F(t)$ of the evolved state using the variational-based CD drivings: $\mathcal{H}^{(1)}(t)$ (dash-dotted green); $\mathcal{H}^{(2)}(t)$ (dashed orange); and $\mathcal{H}^{(3)}(t)$ (solid blue), respectively. As a contrast, the native protocol using $\mathcal{H}_0(t)$ is also described (dotted black). Here we adopt the linear ramp $J_1(t) = \frac{t}{T}, J_2(t) = 1 - \frac{t}{T}$ with $T = 1$.

operators $\mathcal{H}_{cd}^{(2)} = \sum_{k=1}^2 \tilde{\alpha}_k^{(2)} \mathcal{L}_i$ can make the final fidelity almost unit (orange dashed line).

Despite taking a rather simple form, it is still challenging to realize $\mathcal{H}_{cd}^{(l)}(t)$ with physically available interactions when we return back to the full Hilbert space, which always involves highly nonlocal many-body operators and time-dependent control of the couplings within the spin chain. To tackle these issues, we will present the feasible and resource-saving shortcuts based on the variational results in combination with two different methods: Floquet engineering and unitary transformation.

A. Floquet engineering

Floquet engineering [52–54] provides an attractive route to quantum state manipulation, especially in the complex many-body systems. Recently, the idea of exploiting Floquet engineering, periodically modulating the parameters in H_0 to effectively mimic the dynamics of CD driving, was proposed [43,55–57], which could enable the need for the complicated terms (not existing in the original quantum system) get canceled. Notice that $\mathcal{H}_{cd}^{(3)}(t)$ is proportional to the commutator of $\boldsymbol{\sigma}_1 \boldsymbol{\sigma}_2$ and $\boldsymbol{\sigma}_2 \boldsymbol{\sigma}_3$, i.e.,

$$
\begin{aligned}
\mathcal{H}_{cd}^{(3)} &= \tilde{\alpha}^{(3)}(t) \sum_{k=1}^3 \mathcal{L}_k \\
&= \frac{\dot{\tilde{J}}_1 \tilde{J}_2 - \dot{\tilde{J}}_2 \tilde{J}_1}{8(\tilde{J}_1^2 - \tilde{J}_1 \tilde{J}_2 + \tilde{J}_2^2)} \frac{i}{2} [\boldsymbol{\sigma}_1 \boldsymbol{\sigma}_2, \, \boldsymbol{\sigma}_2 \boldsymbol{\sigma}_3],
\end{aligned} \qquad (24)
$$

which indicates $\mathcal{H}_{cd}^{(3)}$ can be effectively constructed by rapidly modulating interactions $\tilde{J}_{1,2}$ in Eq. (9). According to the general procedure in Ref. [55], $\mathcal{H}_{cd}^{(3)}$ can be approximately realized by

$$\mathcal{H}_{Fcd} = c_1(t) \boldsymbol{\sigma}_1 \boldsymbol{\sigma}_2 + c_2(t) \boldsymbol{\sigma}_2 \boldsymbol{\sigma}_3, \qquad (25)$$

with the control functions $c_{1,2}(t)$ taking the form of a truncated Fourier series

$$\sum_l [\mathcal{A}_l \sin(l\omega t) + \mathcal{B}_l \cos(l\omega t)]. \qquad (26)$$

Here ω, l are the fundamental frequency, truncated term, respectively, and $\{\mathcal{A}_l, \mathcal{B}_l\}$ denote the undetermined parameters. According to the Magnus expansion (ME) [58], the propagator of some Hamiltonian $\tilde{H}(t)$ can be represented as $U(t) = \exp[\Omega(t)]$ with a series expansion $\Omega(t) =$

$\Omega^1(t) + \Omega^2(t) + \cdots$, and the first two terms read

$$\Omega^1(t) = -\frac{i}{\hbar} \int_0^t \tilde{H}(t_1) dt_1,$$

$$\Omega^2(t) = \frac{1}{2}\left(\frac{-i}{\hbar}\right)^2 \int_0^t dt_1 \int_0^{t_1} dt_2 [\tilde{H}(t_1), \tilde{H}(t_2)]. \quad (27)$$

To reproduce the CD evolution driven by $\mathcal{H}_{cd}^{(3)}$, the evolution time T will be divided into N_t periods with the duration $\tau = T/N_t = 2\pi/\omega$. During each period, the MEs for the propagators generated by $\mathcal{H}_{cd}^{(3)}$ and $\mathcal{H}_{Fcd}$, respectively, should coincide up to a desired order in τ. Here the first-order approximation of ME induced by $\mathcal{H}_{cd}^{(3)}$ in the nth period is

$$\Omega_{cd}(\tau) = -i\tau \tilde{\alpha}^{(3)}(\tau/2) \sum_{k=1}^3 \mathcal{L}_k + O(\tau^3). \quad (28)$$

For simplicity, the control functions $c_{1,2}(t)$ in Eq. (25) can be chosen as

$$c_1(t) = \mathcal{A}\sqrt{\omega}\cos(\omega t), \quad c_2(t) = \mathcal{B}\sqrt{\omega}\sin(\omega t). \quad (29)$$

The amplitudes of $c_{1,2}(t)$ are in proportion to $\sqrt{\omega}$, which makes the second term of ME to be of first order in τ [55]. The first terms of ME generated by $\mathcal{H}_{Fcd}$ in the nth period read

$$\Omega_{Fcd}(\tau) = -i\tau \mathcal{A}\mathcal{B} \sum_{k=1}^3 \mathcal{L}_k + O(\tau^{3/2}). \quad (30)$$

To ensure $M_{cd}(\tau) \approx M_F(\tau)$ at all the periods, the constraint $\mathcal{A}\mathcal{B} = \tilde{\alpha}^{(3)}(t)$ for the small τ is imposed. When the original sweep functions vary monotonically, e.g., $J_1(t) = \frac{t}{T}$ and $J_2(t) = 1 - \frac{t}{T}$, the coefficient $\tilde{\alpha}^{(3)}(t)$ will keep positive. A possible solution of the constraint equation above is

$$\mathcal{A}(t) = \mathcal{B}(t) = \sqrt{\tilde{\alpha}^{(3)}(t)}, \quad (31)$$

and thus Eq. (25) turns to

$$\mathcal{H}_{Fcd}(t) = \sqrt{\omega \tilde{\alpha}^{(3)}}[\cos(\omega t)\boldsymbol{\sigma}_1\boldsymbol{\sigma}_2 + \sin(\omega t)\boldsymbol{\sigma}_2\boldsymbol{\sigma}_3]. \quad (32)$$

Subsequently, the variational-based CD driving $\mathcal{H}^{(3)}(t)$ can be approximately constructed by

$$\mathcal{H}^F = \mathcal{H}_0 + \mathcal{H}_{Fcd}$$
$$= \mathcal{J}_1(t)\boldsymbol{\sigma}_1\boldsymbol{\sigma}_2 + \mathcal{J}_2(t)\boldsymbol{\sigma}_2\boldsymbol{\sigma}_3, \quad (33)$$

with the time-dependent couplings

$$\begin{cases} \mathcal{J}_1 = \tilde{J}_1 + \sqrt{\omega \tilde{\alpha}^{(3)}}\cos(\omega t), \\ \mathcal{J}_2 = \tilde{J}_2 + \sqrt{\omega \tilde{\alpha}^{(3)}}\sin(\omega t). \end{cases} \quad (34)$$

As the Floquet-driving Hamiltonian (33) has the same structure with the original Hamiltonian (9), the adiabatic quantum-state transfer will be accelerated with no need for auxiliary CD terms when the full Hilbert space is revived. It is remarkable that Ref. [43] also provides an alternative strategy for constructing Floquet-engineering counterdiabatic protocols.

Figure 3 displays the instantaneous infidelity $1 - F(t)$ of the evolved state governed by the Floquet Hamiltonian $\mathcal{H}^F(t)$ when $\omega = 20\pi$, 40π, and 80π, respectively. Compared with
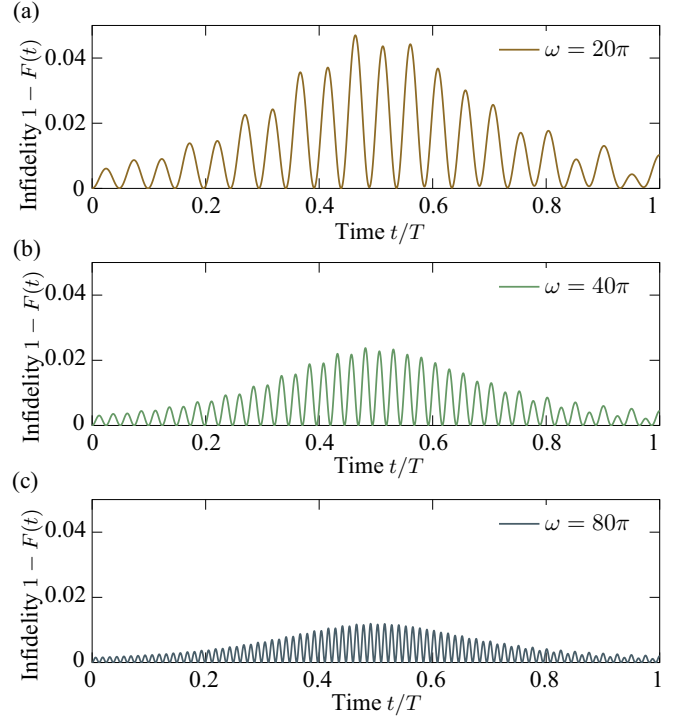

(a)

(b)

(c)

FIG. 3. Instantaneous infidelity $1 - F(t)$ for the Floquet-engineering protocol obtained by Eq. (34), with $\omega = 20\pi$ (top), 40π (middle), and 80π (bottom). The initial sweep functions are set as $J_1(t) = \frac{t}{T}, J_2(t) = 1 - \frac{t}{T}$ with $T = 1$.

the fidelity using the original adiabatic scheme (see Fig. 2 for details), the fidelity can always keep a high level. For instance, a final fidelity around 0.99 can be achieved in the case of $\omega = 20\pi$. There is a slight deviation in the vicinity of the middle part, as the energy gap tends to close, and thus, the suppression for nonadiabatic transitions gets weakened. To achieve a higher-precise dynamics simulation, we can improve the sampling rates by increasing ω. As shown in Figs. 3(b) and 3(c), when the oscillating frequency ω increases up to 40π or 80π, the undesired transitions can be further eliminated. Nevertheless, it should be noted that $\mathcal{H}_{Fcd}$ is proportional to $\sqrt{\omega}$, i.e., higher-precise dynamics here are obtained with the stronger qubit-chain couplings. Therefore, choosing an appropriate ω will involve a trade-off between a desired control precision and the validity of weak-coupling condition in Sec. II.

B. Unitary transformation

An alternative to construct feasible shortcuts from existing CD protocols is to perform suitable unitary transformations, which has been explored with different methods such as multiple Schrödinger dynamics [59], dressed states [60], and Lie transformation [61]. For multilevel systems, however, obtaining analytic unitary transformations is still intractable. We remark that the assisted CD term $\mathcal{H}_{cd}^{(2)} = \sum_{i=1}^2 \tilde{\alpha}_i^{(2)}\mathcal{L}_i$ also provides almost perfect transitionless driving as shown in Fig. 2. Meanwhile, inspired by the work [22,35,62], here we apply the unitary transformation $\mathcal{U}(t) = \prod_{i=1}^2 e^{-i\gamma_i(t)\sigma_i^z\sigma_{i+1}^z}$ on

the variational-based CD shortcut

$$\mathcal{H}^{(2)} = \mathcal{H}_0 + \mathcal{H}_{\mathrm{cd}}^{(2)}. \qquad (35)$$

$$\mathcal{H}^{U} = (\tilde{J}_1 + \dot{\gamma}_1)\sigma_1^z\sigma_2^z + (\tilde{J}_2 + \dot{\gamma}_2)\sigma_2^z\sigma_3^z + (\sigma_1^x\sigma_2^x + \sigma_1^y\sigma_2^y)\big[\tilde{J}_1\cos 2\gamma_2 - \alpha_1^{(2)}\sin 2\gamma_2\big] + (\sigma_2^x\sigma_3^x + \sigma_2^y\sigma_3^y)\big[\tilde{J}_2\cos 2\gamma_1 + \alpha_2^{(2)}\sin 2\gamma_1\big]$$
$$+ \big(\sigma_1^x\sigma_2^y\sigma_3^z - \sigma_1^y\sigma_2^x\sigma_3^z\big)\big[\alpha_1^{(2)}\cos 2\gamma_2 + \tilde{J}_1\sin 2\gamma_2\big] + \big(\sigma_1^z\sigma_2^x\sigma_3^y - \sigma_1^z\sigma_2^y\sigma_3^x\big)\big[\tilde{J}_2\sin 2\gamma_1 - \alpha_2^{(2)}\cos 2\gamma_1\big]. \qquad (36)$$

The three-body interactions are undesirable; we can eliminate these terms by making $\gamma_{1,2}(t)$ meet the following constraints

$$\tilde{J}_2\sin 2\gamma_1 = \alpha_2^{(2)}\cos 2\gamma_1, \quad \tilde{J}_1\sin 2\gamma_2 = -\alpha_1^{(2)}\cos 2\gamma_2, \qquad (37)$$

and thus, we have

$$\gamma_1(t) = \frac{1}{2}\arctan\frac{\alpha_2^{(2)}}{\tilde{J}_2}, \quad \gamma_2(t) = -\frac{1}{2}\arctan\frac{\alpha_1^{(2)}}{\tilde{J}_1}. \qquad (38)$$

The wave functions and Hamiltonians in the two reference frames will coincide at the boundary times if $\mathcal{U}(0) = \mathcal{U}(T) = 1$ and $\dot{\mathcal{U}}(0) = \dot{\mathcal{U}}(T) = 0$, which mean the condition

$$\gamma_{1,2}(0) = \gamma_{1,2}(T) = \dot{\gamma}_{1,2}(0) = \dot{\gamma}_{1,2}(T) = 0 \qquad (39)$$

should be satisfied. Deduced from Eq. (38), $\gamma_{1,2}(t)$ at the initial and final times can be described as

$$\begin{cases} \gamma_1(0) = \dfrac{1}{2}\arctan\dfrac{\dot{\tilde{J}}_1(0)}{8}, \quad \gamma_1(T) = \lim_{t\to T}\dfrac{1}{2}\arctan\dfrac{-\dot{\tilde{J}}_2}{4\tilde{J}_2}, \\[3mm] \gamma_2(0) = \lim_{t\to 0}\dfrac{1}{2}\arctan\dfrac{-\dot{\tilde{J}}_1}{4\tilde{J}_1}, \quad \gamma_2(T) = \dfrac{1}{2}\arctan\dfrac{\dot{\tilde{J}}_2(T)}{8}, \end{cases} \qquad (40)$$

Then, the unitarily equivalent Hamiltonian in the new rotation frame reads

and the first-order derivatives at boundaries are

$$\begin{cases} \dot{\gamma}_1(0) = \dfrac{4\ddot{\tilde{J}}_1(0) + 6\dot{\tilde{J}}_1^2(0) - 12\dot{\tilde{J}}_1(0)\dot{\tilde{J}}_2(0)}{\dot{\tilde{J}}_1^2(0) + 64}, \quad \dot{\gamma}_1(T) = 2, \\[3mm] \dot{\gamma}_2(0) = 2, \quad \dot{\gamma}_2(T) = \dfrac{4\ddot{\tilde{J}}_2(T) + 6\dot{\tilde{J}}_2^2(T) - 12\dot{\tilde{J}}_2(T)\dot{\tilde{J}}_1(T)}{\dot{\tilde{J}}_2^2(T) + 64}. \end{cases} \qquad (41)$$

Equations (40) and (41) depend on the concrete forms of $\tilde{J}_{1,2}(t)$, or rather $J_{1,2}(t)$, considering the relationship between them in Eq. (10). Obviously, the condition in Eq. (39) is inconsistent, and thus the desired unitary transformation is impracticable.

To achieve our goal, we can make the first-order and second-order derivatives of $J_{1,2}(t)$ follow the boundary constraints

$$\dot{J}_1(0) = \ddot{J}_1(0) = 0, \quad \dot{J}_2(T) = \ddot{J}_2(T) = 0. \qquad (42)$$

Consequently, the two wave functions in different reference frames will be equivalent at the boundary times except for global phases, i.e.,

$$\begin{cases} \mathcal{U}(0)|\Phi(0)\rangle = e^{-i\frac{\pi}{4}}|\Phi(0)\rangle, \\[2mm] \mathcal{U}(T)|\Phi(T)\rangle = e^{i\frac{\pi}{4}}|\Phi(T)\rangle. \end{cases} \qquad (43)$$

Here the global phase has no impact on our goal. Furthermore, under the conditions in Eq. (42) we can easily obtain the
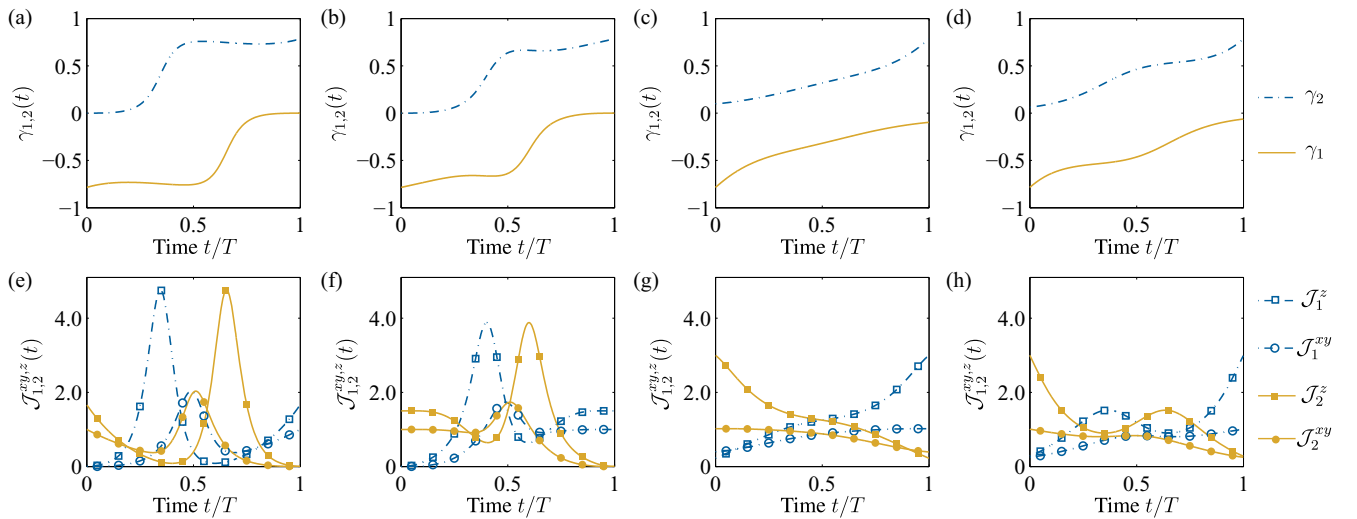

FIG. 4. The parameters $\gamma_{1,2}(t)$ and $\mathcal{J}_{1,2}^{xy,z}(t)$ in Eq. (46) with the different ramps (from left to right): 1. $J_1 = \frac{t^3}{T^3}, J_2(t) = (1 - \frac{t}{T})^3$; 2. $J_1 = \sin^2[\frac{\pi}{2}\sin^2(\frac{\pi t}{2T})], J_2 = 1 - J_1$; 3. $J_1 = \sin\frac{\pi t}{2T}, J_2 = \cos\frac{\pi t}{2T}$; 4. $J_1 = \frac{t}{T}, J_2 = 1 - \frac{t}{T}$. In all panels $T = 1$. Notice that $\gamma_{1,2}(t)$ are taken in the interval $[-\frac{\pi}{4}, \frac{\pi}{4}]$ regardless of their periodicities.
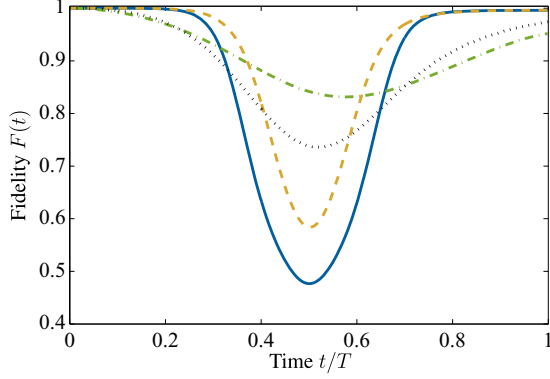
FIG. 5. The instantaneous fidelity $F(t)$ of the unitarily equivalent scheme [Eq. (45)] using four sets of sweep functions shown in Fig. 4 for $T = 1$. A detailed description is given in the main text.

following commuting relations:

$$[\mathcal{H}^{\mathrm{U}}(0), \mathcal{H}^{(2)}(0)] = 0, \quad [\mathcal{H}^{\mathrm{U}}(T), \mathcal{H}^{(2)}(T)] = 0, \quad (44)$$

which indicate the Hamiltonians in the two reference frames share common eigenstates at the boundaries. To summarize, the unitarily equivalent Hamiltonian in Eq. (36) becomes

$$\mathcal{H}^{\mathrm{U}} = \mathcal{J}_1^{xy}(t)\left(\sigma_1^x\sigma_2^x + \sigma_1^y\sigma_2^y\right) + \mathcal{J}_1^z(t)\sigma_1^z\sigma_2^z$$
$$+ \mathcal{J}_2^{xy}(t)\left(\sigma_2^x\sigma_3^x + \sigma_2^y\sigma_3^y\right) + \mathcal{J}_2^z(t)\sigma_2^z\sigma_3^z, \quad (45)$$

with the time-dependent couplings

$$\begin{cases} \mathcal{J}_1^{xy} = \tilde{J}_1\cos 2\gamma_2 - \alpha_1^{(2)}\sin 2\gamma_2, & \mathcal{J}_1^z = \tilde{J}_1 + \dot{\gamma}_1, \\ \mathcal{J}_2^{xy} = \tilde{J}_2\cos 2\gamma_1 + \alpha_2^{(2)}\sin 2\gamma_1, & \mathcal{J}_2^z = \tilde{J}_2 + \dot{\gamma}_2. \end{cases} \quad (46)$$

Since the designed $\mathcal{H}^{\mathrm{U}}$ does not introduce operators not included in $\mathcal{H}_0$, we only need to manipulate the qubit-chain couplings, which will facilitate the experimental realization.

Then, based on Eq. (42), different driving protocols can be designed. Here, we choose the polynomial functions

$$J_1(t) = \frac{t^3}{T^3}, \quad J_2(t) = \left(1 - \frac{t}{T}\right)^3, \quad (47)$$

and the trigonometric functions

$$J_1(t) = \sin^2\left[\frac{\pi}{2}\sin^2\left(\frac{\pi t}{2T}\right)\right], \quad J_2(t) = 1 - J_1. \quad (48)$$

The corresponding parameters $\gamma_{1,2}$ and $\mathcal{J}_{1,2}^{xy,z}$ when $T = 1$ are illustrated in Figs. 4(a), 4(e) and Figs. 4(b) and 4(f). For the latter sweep, both $\dot{J}_{1,2}(t)$ and $\ddot{J}_{1,2}(t)$ are zero at the beginning and end of the protocol, far beyond the constraints in Eq. (42), which brings out a smooth change of $\mathcal{J}_{1,2}^{xy,z}$ near the initial and final times.

The instantaneous fidelities $F(t)$ are presented in Fig. 5 where the initial state $|\Phi(0)\rangle$ is driven by $\mathcal{H}^{\mathrm{U}}$ with the polynomial functions (47) (blue solid line) and trigonometric functions (48) (orange dashed line), respectively. The result shows a high-fidelity quantum state manipulation can be realized via the unitarily equivalent shortcuts. In the middle time $\mathcal{H}^{\mathrm{U}}$ does not equal to $\mathcal{H}^{(2)}$, so the instantaneous fidelity $F(t)$ will decrease first and then increase. It is noteworthy that at

the final time the fidelity, though close to 1, can only reach the value as same as the one using the shortcut $\mathcal{H}^{(2)}$. If the original sweeps $J_{1,2}(t)$ do not satisfy the boundary conditions, the final fidelity will decrease obviously. As a contrast, Fig. 5 also presents $F(t)$ for the ramps $J_1(t) = \sin\frac{\pi t}{2T}$, $J_2(t) = \cos\frac{\pi t}{2T}$ (green dash-dotted line) and $J_1(t) = \frac{t}{T}$, $J_2(t) = 1 - \frac{t}{T}$ (black dotted line), respectively; see Figs. 4(c) and 4(d) and Figs. 4(g) and 4(h) for a detailed description of $\gamma_{1,2}$ and $\mathcal{J}_{1,2}^{xy,z}$. Under the same condition, the final fidelities reach merely about 0.95 and 0.97, respectively. If we increase T, $\dot{J}_{1,2}$ tend to zero at the boundary times. It makes Eq. (42) hold approximately and the final fidelity as same as that using sweep functions (47) or (48) will be achieved.

IV. NUMERICAL RESULTS

To show the validity of the two constructed shortcuts derived from the variational-based CD approach, we map from the effective model back to the whole spin chain by substituting the marginal couplings with the Eqs. (34) and (46) in the Hamiltonian (6), respectively, and explore the dynamical evolution numerically. For simplicity, we employ Eq. (48) as the initial adiabatic drivings and assess the QST fidelity $\mathcal{F}$ with respect to T

$$\mathcal{F}(T) = \langle\psi_0|\rho_f(T)|\psi_0\rangle. \quad (49)$$

Here $|\psi_0\rangle$ is the target state and $\rho_f(T)$ stands for the reduced density matrix of the receiver spin by tracing out all the others subsystems, i.e.,

$$\rho_f(T) = \mathrm{Tr}_{\bar{\mathrm{R}}}[U(0, T)|\Psi(0)\rangle\langle\Psi(0)|U^\dagger(0, T)], \quad (50)$$

with $|\Psi(0)\rangle$ being the initial state of the whole system and $U(0, T)$ being the evolution operator from time $t = 0$ to T with the new designed protocols.

In Fig. 6, we plot the QST fidelity $\mathcal{F}(T)$ (lines with symbols) via the Floquet-engineering and unitarily equivalent shortcuts, respectively. For different-size Heisenberg chains, $\mathcal{F}(T)$ rise up quickly and then maintain a high level for both designed strategies. Since the minimum energy gap between the ground and first excited states decreases with the growth of system size, it will take a longer time to reach the same level for larger systems. If using the original adiabatic scheme (lines without symbols), the desired state transfer occurs until T is large enough to satisfy the adiabatic condition. For instance, to achieve a QST fidelity of $\mathcal{F} > 0.99$ across the $N = 7$ spin chain, the minimal evolution time of both shortcuts will be at least an order of magnitude less than that of the adiabatic protocol. However, the shorter the evolution time is, the larger the qubit-chain couplings in Eqs. (34) and (46) require. Therefore, the weak-coupling condition becomes invalid as T continues to decrease, which accounts for a dramatic drop of $\mathcal{F}$ in both shortcuts. In addition, compared to the unitarily equivalent scheme, the Floquet-engineering shortcut has larger qubit-chain couplings for a short duration T, which gives rise to a lower fidelity at the beginning in Fig. 6(a).

To further demonstrate the robustness of the designed protocols, we choose $N = 5$ spin channel without loss of generality and numerically investigate the resilience with respect to the errors from the control fields and the evolution time.
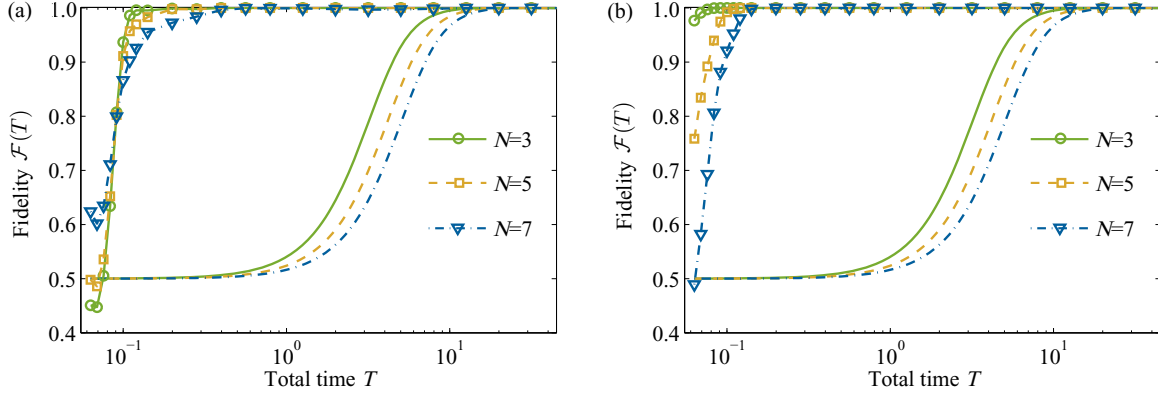
FIG. 6. QST fidelity $\mathcal{F}(T)$ using (a) Floquet-engineering shortcut [Eq. (34)] and (b) unitarily equivalent shortcut [Eq. (46)] for $N = 3, 5,$ 7 spin chain. The lines marked with symbols denote the speed-up results, and the lines without symbols are the adiabatic results. Here we set $J_0 = 70$, $\omega = 20\pi$ and choose the original driving protocol having the form of Eq. (48).

A. Errors of control fields

Here we assume that the errors of time-dependent control fields mainly come from the imperfections in amplitudes of the two fringe couplings

$$\mathcal{J}_i = \mathcal{J}_i + \delta\mathcal{J}_i, \quad (i = 1, 2). \tag{51}$$

As shown in Figs. 7(a) and 7(b) for $T = 0.5$, even if the relative errors $\zeta_{\mathcal{J}_i} = |\delta\mathcal{J}_i/\mathcal{J}_i| = 15\%$, both shortcuts can achieve a fidelity of $\mathcal{F} > 0.99$. It manifests that our speed-up schemes are robust against the amplitudes errors. In practice, it is hard to create a desired spin channel by precisely manipulating the couplings between spins based on artificial structures. Anderson localization due to this inevitable disorder will limit state
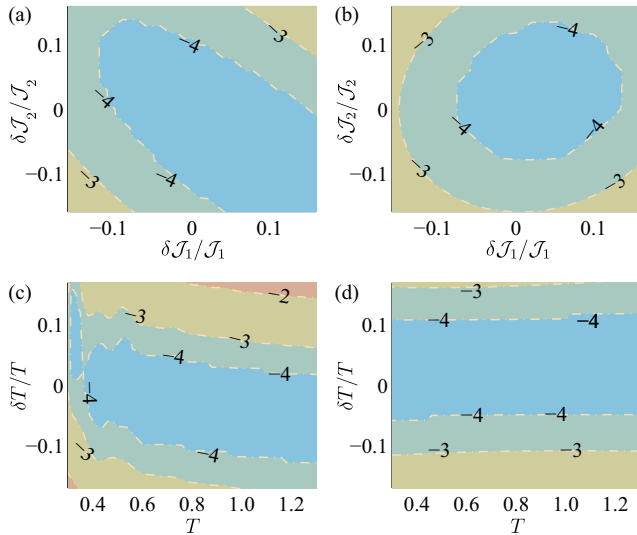

FIG. 7. (a), (b) The logarithm of infidelity $\log_{10}(1 - \mathcal{F})$ versus the imperfections of the control fields. (c), (d) The logarithm of infidelity $\log_{10}(1 - \mathcal{F})$ versus the errors of evolution time. The subfigures in the left and right columns denote the results of Floquet-engineering and unitarily equivalent shortcuts [Eqs. (34) and (46)], respectively. The values of contour lines are labeled in each subfigure. Here we set $J_0 = 70$, $\omega = 20\pi$, and use trigonometric ramp [Eq. (47)].

transfer beyond a distance in the chain [63]. Nevertheless, the spin channel with the strong couplings here still behaves as an effective 1/2 spin, even if random static variations exist, and thus the quantum information transfer across a large distance [64].

B. Errors of evolution time

The robustness of our schemes against time errors is also investigated. As displayed in Figs. 7(c) and 7(d), we numerically calculate the final fidelity $\mathcal{F}$ of the evolved state via the two shortcuts, where deviation δT is added to the total evolution time, i.e.,

$$T = T + \delta T. \tag{52}$$

We set the maximum relative deviation $\zeta_T = |\delta T/T| = 15\%$ for different T and find that the fidelity $\mathcal{F}$ using the two speed-up schemes can still exceed 0.99 in most situations. If we transfer the target state as fast as possible i.e., $T \to 0$, the infidelity, originating from imperfectly mapping to the effective three-spin model, would take place obviously, as the inner coupling of spin chain is finite in practice. The higher-order approximation should be introduced into the effective Hamiltonian (9), e.g., the direct interaction between the sender and receiver [51] and it will be left for future research.

V. CONCLUSION

High-fidelity and fast information transfer between two distant parties is of importance in quantum computation and quantum communication. To this end, we propose two alternative schemes to speed up the adiabatic state transfer across a one-dimensional odd-size Heisenberg spin chain with strong couplings. On one hand, by exploiting an simplified Hamiltonian in the subspace spanned by the ground doublet states of the odd-size chain and the states of externally coupled qubits, the optimal transitionless passages are effectively constructed by virtue of the variational principle to CD driving, without the need for the diagonalization of the Hamiltonian. On the other hand, combined with Floquet driving and unitary transformation, two feasible protocols derived from the existed variational results are constructed, respectively. Both the

speed-up protocols only require the control of the marginal qubit-chain couplings, which can greatly reduce the difficulty of physical implementations in practice.

Numerical simulation confirms that our designed shortcuts allow for high-fidelity and robust quantum state transfer despite not being in the adiabatic limit, which provide potential applications for multi-spin systems, such as quantum dots [16] and ultracold atoms [48]. In the future we may explore the influence of high-order approximation [51] in Eq. (9) when the couplings within the chain are not strong enough and design the possible shortcuts for perfect and fast QST. In addition, extending these results to the transportation of two-qubit states [65,66], e.g., the Bell state, could also be considered.

[1] M. A. Nielsen and I. L. Chuang, *Quantum Computation and Quantum Information: 10th Anniversary Edition*, 10th ed. (Cambridge University Press, Cambridge, 2011).

[2] S. Bose, Quantum communication through spin chain dynamics: An introductory overview, Contemp. Phys. **48**, 13 (2007).

[3] S. Bose, Quantum Communication through an Unmodulated Spin Chain, Phys. Rev. Lett. **91**, 207901 (2003).

[4] M. Friesen, A. Biswas, X. Hu, and D. Lidar, Efficient Multiqubit Entanglement via a Spin Bus, Phys. Rev. Lett. **98**, 230503 (2007).

[5] L.-A. Wu, Y.-X. Liu, and F. Nori, Universal existence of exact quantum state transmissions in interacting media, Phys. Rev. A **80**, 042315 (2009).

[6] S. Paganelli, S. Lorenzo, T. J. G. Apollaro, F. Plastina, and G. L. Giorgi, Routing quantum information in spin chains, Phys. Rev. A **87**, 062309 (2013).

[7] S. Oh, Y.-P. Shim, J. Fei, M. Friesen, and X. Hu, Resonant adiabatic passage with three qubits, Phys. Rev. A **87**, 022332 (2013).

[8] S. Ashhab, Quantum state transfer in a disordered one-dimensional lattice, Phys. Rev. A **92**, 062305 (2015).

[9] Z.-M. Wang, M. S. Sarandy, and L.-A. Wu, Almost exact state transfer in a spin chain via pulse control, Phys. Rev. A **102**, 022601 (2020).

[10] V. Balachandran and J. Gong, Adiabatic quantum transport in a spin chain with a moving potential, Phys. Rev. A **77**, 012303 (2008).

[11] G. Della Valle, M. Ornigotti, T. T. Fernandez, P. Laporta, S. Longhi, A. Coppa, and V. Foglietti, Adiabatic light transfer via dressed states in optical waveguide arrays, Appl. Phys. Lett. **92**, 011106 (2008).

[12] L. M. Jong, A. D. Greentree, V. I. Conrad, L. C. L. Hollenberg, and D. N. Jamieson, Coherent tunneling adiabatic passage with the alternating coupling scheme, Nanotechnology **20**, 405402 (2009).

[13] S. Longhi, Coherent transfer by adiabatic passage in two-dimensional lattices, Ann. Phys. **348**, 161 (2014).

[14] U. Farooq, A. Bayat, S. Mancini, and S. Bose, Adiabatic many-body state preparation and information transfer in quantum dot arrays, Phys. Rev. B **91**, 134303 (2015).

[15] M. J. Gullans and J. R. Petta, Coherent transport of spin by adiabatic passage in quantum dot arrays, Phys. Rev. B **102**, 155404 (2020).

[16] Y. P. Kandel, H. Qiao, S. Fallahi, G. C. Gardner, M. J. Manfra, and J. M. Nichol, Adiabatic quantum state transfer in a semiconductor quantum-dot spin chain, Nat. Commun. **12**, 2156 (2021).

[17] M. V. Berry, Transitionless quantum driving, J. Phys. A: Math. Theor. **42**, 365303 (2009).

[18] M. Demirplak and S. A. Rice, Adiabatic population transfer with control fields, J. Phys. Chem. A **107**, 9937 (2003).

[19] A. del Campo, Shortcuts to Adiabaticity by Counterdiabatic Driving, Phys. Rev. Lett. **111**, 100502 (2013).

[20] D. Guéry-Odelin, A. Ruschhaupt, A. Kiely, E. Torrontegui, S. Martínez-Garaot, and J. G. Muga, Shortcuts to adiabaticity: Concepts, methods, and applications, Rev. Mod. Phys. **91**, 045001 (2019).

[21] A. del Campo and K. Kim, Focus on Shortcuts to Adiabaticity, New J. Phys. **21**, 050201 (2019).

[22] R. R. Agundez, C. D. Hill, L. C. L. Hollenberg, S. Rogge, and M. Blaauboer, Superadiabatic quantum state transfer in spin chains, Phys. Rev. A **95**, 012317 (2017).

[23] A. Baksic, R. Belyansky, H. Ribeiro, and A. A. Clerk, Shortcuts to adiabaticity in the presence of a continuum: Applications to itinerant quantum state transfer, Phys. Rev. A **96**, 021801(R) (2017).

[24] X. Shi, H. Yuan, X. Mao, Y. Ma, and H. Q. Zhao, Robust quantum state transfer inspired by Dzyaloshinskii-Moriya interactions, Phys. Rev. A **95**, 052332 (2017).

[25] B.-H. Huang, Y.-H. Kang, Y.-H. Chen, Z.-C. Shi, J. Song, and Y. Xia, Quantum state transfer in spin chains via shortcuts to adiabaticity, Phys. Rev. A **97**, 012333 (2018).

[26] Z.-M. Wang, C. A. Bishop, J. Jing, Y.-J. Gu, C. Garcia, and L.-A. Wu, Shortcut to nonadiabatic quantum state transmission, Phys. Rev. A **93**, 062338 (2016).

[27] Y. Chen, L. Zhang, Y. Gu, and Z.-M. Wang, Acceleration of adiabatic quantum state transfer in a spin chain under zero-energy-change pulse control, Phys. Lett. A **382**, 2795 (2018).

[28] F. M. D'Angelis, F. A. Pinheiro, D. Guéry-Odelin, S. Longhi, and F. Impens, Fast and robust quantum state transfer in a topological Su-Schrieffer-Heeger chain with next-to-nearest-neighbor interactions, Phys. Rev. Research **2**, 033475 (2020).

[29] A. Kiely and S. Campbell, Fast and robust magnon transport in a spin chain, New J. Phys. **23**, 033033 (2021).

[30] N. E. Palaiodimopoulos, I. Brouzos, F. K. Diakonos, and G. Theocharis, Fast and robust quantum state transfer via a topological chain, Phys. Rev. A **103**, 052409 (2021).

[31] A. del Campo, M. M. Rams, and W. H. Zurek, Assisted Finite-Rate Adiabatic Passage Across a Quantum Critical Point: Exact Solution for the Quantum Ising Model, Phys. Rev. Lett. **109**, 115703 (2012).

[32] S. Campbell, G. De Chiara, M. Paternostro, G. M. Palma, and R. Fazio, Shortcut to Adiabaticity in the Lipkin-Meshkov-Glick Model, Phys. Rev. Lett. **114**, 177206 (2015).

[33] T. Opatrný and K. Mølmer, Partial suppression of nonadiabatic transitions, New J. Phys. **16**, 015025 (2014).

[34] Y. Ji, J. Bian, X. Chen, J. Li, X. Nie, H. Zhou, and X. Peng, Experimental preparation of Greenberger-Horne-Zeilinger states in an Ising spin model by partially suppressing the nonadiabatic transitions, Phys. Rev. A **99**, 032323 (2019).

[35] D. Sels and A. Polkovnikov, Minimizing irreversible losses in quantum systems by local counterdiabatic driving, Proc. Natl. Acad. Sci. USA **114**, E3909 (2017).

[36] M. Kolodrubetz, D. Sels, P. Mehta, and A. Polkovnikov, Geometry and non-adiabatic response in quantum and classical systems, Phys. Rep. **697**, 1 (2017).

[37] M. Pandey, P. W. Claeys, D. K. Campbell, A. Polkovnikov, and D. Sels, Adiabatic Eigenstate Deformations as a Sensitive Probe for Quantum Chaos, Phys. Rev. X **10**, 041017 (2020).

[38] T. Hatomura and K. Takahashi, Controlling and exploring quantum systems by algebraic expression of adiabatic gauge potential, Phys. Rev. A **103**, 012220 (2021).

[39] A. Hartmann and W. Lechner, Rapid counter-diabatic sweeps in lattice gauge adiabatic quantum computing, New J. Phys. **21**, 043025 (2019).

[40] G. Passarelli, V. Cataudella, R. Fazio, and P. Lucignano, Counterdiabatic driving in the quantum annealing of the *p*-spin model: A variational approach, Phys. Rev. Research **2**, 013283 (2020).

[41] L. Prielinger, A. Hartmann, Y. Yamashiro, K. Nishimura, W. Lechner, and H. Nishimori, Two-parameter counter-diabatic driving in quantum annealing, Phys. Rev. Research **3**, 013227 (2021).

[42] A. Hartmann, G. B. Mbeng, and W. Lechner, Polynomial scaling enhancement in ground-state preparation of Ising spin models via counter-diabatic driving, Phys. Rev. A **105**, 022614 (2022).

[43] P. W. Claeys, M. Pandey, D. Sels, and A. Polkovnikov, Floquet-Engineering Counterdiabatic Protocols in Quantum Many-Body Systems, Phys. Rev. Lett. **123**, 090602 (2019).

[44] H. Zhou, Y. Ji, X. Nie, X. Yang, X. Chen, J. Bian, and X. Peng, Experimental Realization of Shortcuts to Adiabaticity in a Nonintegrable Spin Chain by Local Counterdiabatic Driving, Phys. Rev. Applied **13**, 044059 (2020).

[45] N. N. Hegade, K. Paul, Y. Ding, M. Sanz, F. Albarrán-Arriagada, E. Solano, and X. Chen, Shortcuts to Adiabaticity in Digitized Adiabatic Quantum Computing, Phys. Rev. Applied **15**, 024038 (2021).

[46] S. Kumar, S. Sharma, and V. Tripathi, Counterdiabatic route for preparation of state with long-range topological order, Phys. Rev. B **104**, 245113 (2021).

[47] F. A. Zwanenburg, A. S. Dzurak, A. Morello, M. Y. Simmons, L. C. L. Hollenberg, G. Klimeck, S. Rogge, S. N. Coppersmith, and M. A. Eriksson, Silicon quantum electronics, Rev. Mod. Phys. **85**, 961 (2013).

[48] P. N. Jepsen, J. Amato-Grill, I. Dimitrova, W. W. Ho, E. Demler, and W. Ketterle, Spin transport in a tunable Heisenberg model realized with ultracold atoms, Nature (London) **588**, 403 (2020).

[49] R. Fazio and H. van der Zant, Quantum phase transitions and vortex dynamics in superconducting networks, Phys. Rep. **355**, 235 (2001).

[50] S. Oh, L.-A. Wu, Y.-P. Shim, J. Fei, M. Friesen, and X. Hu, Heisenberg spin bus as a robust transmission line for quantum-state transfer, Phys. Rev. A **84**, 022330 (2011).

[51] S. Oh, M. Friesen, and X. Hu, Even-odd effects of Heisenberg chains on long-range interaction and entanglement, Phys. Rev. B **82**, 140403(R) (2010).

[52] M. Bukov, L. D'Alessio, and A. Polkovnikov, Universal high-frequency behavior of periodically driven systems: From dynamical stabilization to Floquet engineering, Adv. Phys. **64**, 139 (2015).

[53] A. Eckardt, Colloquium: Atomic quantum gases in periodically driven optical lattices, Rev. Mod. Phys. **89**, 011004 (2017).

[54] F. Petiziol, M. Sameti, S. Carretta, S. Wimberger, and F. Mintert, Quantum Simulation of Three-Body Interactions in Weakly Driven Quantum Systems, Phys. Rev. Lett. **126**, 250504 (2021).

[55] F. Petiziol, B. Dive, F. Mintert, and S. Wimberger, Fast adiabatic evolution by oscillating initial Hamiltonians, Phys. Rev. A **98**, 043436 (2018).

[56] E. Boyers, M. Pandey, D. K. Campbell, A. Polkovnikov, D. Sels, and A. O. Sushkov, Floquet-engineered quantum state manipulation in a noisy qubit, Phys. Rev. A **100**, 012341 (2019).

[57] H. Zhou, X. Chen, X. Nie, J. Bian, Y. Ji, Z. Li, and X. Peng, Floquet-engineered quantum state transfer in spin chains, Sci. Bull. **64**, 888 (2019).

[58] S. Blanes, F. Casas, J. Oteo, and J. Ros, The Magnus expansion and some of its applications, Phys. Rep. **470**, 151 (2009).

[59] S. Ibáñez, X. Chen, E. Torrontegui, J. G. Muga, and A. Ruschhaupt, Multiple Schrödinger Pictures and Dynamics in Shortcuts to Adiabaticity, Phys. Rev. Lett. **109**, 100403 (2012).

[60] A. Baksic, H. Ribeiro, and A. A. Clerk, Speeding up Adiabatic Quantum State Transfer by Using Dressed States, Phys. Rev. Lett. **116**, 230503 (2016).

[61] Y.-H. Kang, Y.-H. Chen, Z.-C. Shi, B.-H. Huang, J. Song, and Y. Xia, Pulse design for multilevel systems by utilizing Lie transforms, Phys. Rev. A **97**, 033407 (2018).

[62] K. Takahashi, Transitionless quantum driving for spin systems, Phys. Rev. E **87**, 062117 (2013).

[63] J. Allcock and N. Linden, Quantum Communication beyond the Localization Length in Disordered Spin Chains, Phys. Rev. Lett. **102**, 110501 (2009).

[64] S. Oh, Y.-P. Shim, J. Fei, M. Friesen, and X. Hu, Effect of randomness on quantum data buses of Heisenberg spin chains, Phys. Rev. B **85**, 224418 (2012).

[65] R. Vieira and G. Rigolin, Almost perfect transport of an entangled two-qubit state through a spin chain, Phys. Lett. A **382**, 2586 (2018).

[66] S. Lorenzo, T. J. G. Apollaro, S. Paganelli, G. M. Palma, and F. Plastina, Transfer of arbitrary two-qubit states via a spin chain, Phys. Rev. A **91**, 042321 (2015).